Distributed MPDR Beamforming in Virtual Arrays

Yuri R. Santos, Mateus de L. Filomeno, Wallace A. Martins, Ivo C. S. Junior, and Moisés V. Ribeiro

***Abstract*— This paper extends the distributed minimum power distortionless response (MPDR) beamformer to 3D virtual arrays with heterogeneous node geometries. We first present a system model of cooperative nodes—each with its own arbitrary array—and generalize the distributed MPDR, originally designed for $\lambda/2$-spaced linear arrays, to 3D arrays. We then evaluate beam pattern shape, directivity, beam efficiency, and bit error rate (BER), benchmarking these metrics against the centralized MPDR. Simulations reveal grating lobes for antenna-element spacings larger than $\lambda/2$, but the array gain mitigates their BER impact. The slow convergence speed of the distributed MPDR indicates the necessity of searching for techniques to improve it. With sufficient snapshots, its performance nearly matches centralized MPDR, confirming its promise for practical virtual arrays, including satellite swarms.**

***Keywords*— antenna array, distributed beamforming, virtual array.**

I. Introduction

Low Earth orbit (LEO) megaconstellation of satellites, commonly operating at altitudes between 500 km and 2000 km, have emerged as a transformative paradigm in space communication technology, traditionally dominated by medium Earth orbit (MEO) and geostationary Earth orbit (GEO) satellites. Driven by several advances in miniaturization and cost-effective technologies, private-capital-driven constellations such as Starlink and OneWeb now deliver low-latency links, allowing unprecedented coverage in remote areas and disaster-response situations [1, 2].

When it comes to communicating with terrestrial nodes not originally designed for satellite communications (*e.g.*, smartphones), achieving a proper link budget for high-throughput communications imposes severe constraints on the antenna size of the space segment. However, the costs associated with the launch of satellites with large antenna arrays are extremely high, requiring alternative solutions. In this context, LEO satellite swarms are being considered for communications [3]. These swarms can be configured in a free-flying formation (*i.e.*, wirelessly connected) or a tethered formation (*i.e.*, wired connected) [4]. These swarms may comprise homogeneous or heterogeneous nodes (*i.e.*, satellites), with each satellite equipped with its own array. Through coordinated internode signaling, the arrays of all satellites collectively form a virtual antenna array. Consequently, beamforming techniques can be employed to enhance signal-to-noise ratio (SNR), increase communication capacity, expand coverage, and improve spectral efficiency, among other benefits [3, 5].

Centralized and distributed beamforming can be applied in a virtual antenna array. The centralized beamforming relies on the collected signals from all nodes at a single fusion center, which computes optimal global weights for a high-precision beam. This approach offers great performance but requires wide internode bandwidth, introduces a single point of failure, and scales poorly with an increasing number of nodes. As for the distributed approach, it allows each node to compute and apply its weights based on locally exchanged parameters, effectively reducing raw-data traffic, tolerating individual failures, and scaling well with the problem dimension. However, it requires accurate synchronization among nodes and may result in suboptimal beams compared to centralized solutions.

Motivated by possible future applications in satellite swarms, this paper focuses on the more fundamental problem of designing fully distributed receiver beamforming algorithms for generic virtual antenna arrays. With this in mind, this work builds upon the so-called distributed Capon beamformer, herein named distributed minimum power distortionless response (MPDR), introduced by Chen and Vaidyanathan [6] in the context of $\lambda/2$-uniformly spaced linear virtual arrays comprised of homogeneous nodes. Thus, we extend the distributed MPDR beamforming algorithm to support virtual arrays composed of heterogeneous nodes with arbitrary 3D geometries. In the case of homogeneous nodes, numerical simulations assess the beam pattern and bit error rate (BER) as functions of internode distances (both shorter and longer than $\lambda/2$) and the number of snapshots of the acquired signals. We then evaluate the distributed MPDR for heterogeneous configurations with internode spacing exceeding $\lambda/2$, a typical scenario in possible future applications. Lastly, we compare the distributed and centralized MPDR algorithms. The results confirm the viability of the distributed MPDR in virtual arrays, while highlighting that reducing the number of snapshots—*e.g.*, through more accurate covariance estimation—remains critical for faster convergence.

II. System Model

Consider a virtual antenna array composed of P nodes distributed in three-dimensional space ($\mathbb{R}^3$), as illustrated in Fig. 1. Unlike the geometric structure of the $\lambda/2$-uniformly spaced linear array adopted in [6], this paper does not impose constraints on the spatial arrangement. In this virtual array model, communication latency and synchronization overhead are not explicitly accounted for, *i.e.*, we assume perfect phase,

This research was supported in part by Coordenação de Aperfeiçoamento de Pessoal de Nível Superior (CAPES) under Grant 001, Conselho Nacional de Desenvolvimento Científico e Tecnológico (CNPq) under grants 445958/2024-3 and 314741/2020-8, and Fundação de Amparo à Pesquisa do Estado de Minas Gerais (FAPEMIG) under grant APQ-04623-22.

Yuri R. Santos, Mateus de L. Filomeno, Ivo C. S. Junior, and Moisés V. Ribeiro are with the Electrical Engineering Department, Federal University of Juiz de Fora, Juiz de Fora, MG 36036-900, Brazil, (e-mail: santos.yr@hotmail.com, delimafilomeno@gmail.com, {moises.ribeiro; ivo.junior}@ufjf.br)

Wallace A. Martins is with the Fédération ENAC ISAE-SUPAERO ONERA, Université de Toulouse, France (e-mail: wallace.martins@isae-supaero.fr).

frequency, and timing synchronization among the nodes. The internode communication is modeled by an undirected and connected graph $\mathcal{G} = (\mathcal{V}, \mathcal{E})$, with nodes represented by the vertex set $\mathcal{V} = \{1, \ldots, P\}$ and bidirectional links represented by the edge set $\mathcal{E}$, ensuring information exchange across nodes. Each node $p \in \mathcal{V}$ hosts a subarray of K_p antenna elements, whose geometry is selected from a predefined set comprising one-, two-, or three-dimensional geometries. The total number of elements in the virtual array is $K = \sum_{p=1}^{P} K_p$. The coordinates $(x_{p,\ell}, y_{p,\ell}, z_{p,\ell})$ of the ℓ^{th} element at the p^{th} node are defined on the basis of a global Cartesian coordinate system, whose origin coincides with the origin of the three-dimensional space.

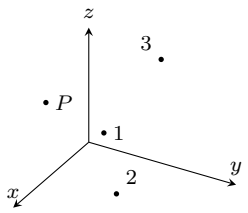

Fig. 1. P nodes distributed in the three-dimensional space.

Let $\{s_m[n]\}$, with $m \in \{1, 2, \cdots, M\}$, denote a set of discrete-time signals transmitted by M sources. We assume that the signal $s_m[n]$ is a realization of a wide-sense stationary (WSS) random sequence $S_m[n]$ satisfying $\mathbb{E}\{S_m[n]\} = 0$, $\mathbb{E}\{S_m[n]S_m^*[n+k]\} = \sigma_{S_m}^2 \delta[k]$, $\mathbb{E}\{S_i[n]S_j^*[n+l]\} = 0$, $i \neq j$, $i, j \in \{1, 2, \ldots, M\}$, with $\mathbb{E}\{\cdot\}$ denoting expectation and $(\cdot)^*$, complex conjugation. Each transmitted signal $s_m[n]$ is composed of symbols that belong to a constellation set $\mathcal{C}_m$. Narrowband array processing is assumed, considering that the waveforms vary slowly in time and space relative to their wavelength.

Let $\mathbf{x}_p[n] = [x_{p,1}[n]\ x_{p,2}[n]\ \cdots\ x_{p,K_p}[n]]^{\mathrm{T}}$ denote the received vector at node p during snapshot n. By concatenating the received vectors from all nodes in the vector $\mathbf{x}[n] = [\mathbf{x}_1^{\mathrm{T}}[n]\ \mathbf{x}_2^{\mathrm{T}}[n]\ \cdots\ \mathbf{x}_P^{\mathrm{T}}[n]]^{\mathrm{T}}$, we can write

$$\mathbf{x}[n] = \mathbf{A}\,\mathbf{s}[n] + \mathbf{v}[n], \tag{1}$$

where $\mathbf{s}[n] = [s_1[n]\ s_2[n]\ \cdots\ s_M[n]]^{\mathrm{T}}$ is the transmitted vector, $\mathbf{A} = [\mathbf{a}_1\ \mathbf{a}_2\ \cdots\ \mathbf{a}_M]$ is the steering matrix associated with the transmitted signals, and $\mathbf{v}[n]$ denotes the noise vector.

The overall steering vector corresponding to the signal from the m^{th} source is defined as $\mathbf{a}_m = [\mathbf{a}_{m,1}^{\mathrm{T}}\ \mathbf{a}_{m,2}^{\mathrm{T}}\ \cdots\ \mathbf{a}_{m,P}^{\mathrm{T}}]^{\mathrm{T}}$, with the p^{th} node's steering vector given by $\mathbf{a}_{m,p} = [a_{m,p,1}\ a_{m,p,2}\ \cdots\ a_{m,p,K_p}]^{\mathrm{T}}$. The phase shift at the $(m,p,\ell)^{\text{th}}$ element is modeled as [7]

$$a_{m,p,\ell} = \mathrm{e}^{-\mathrm{j}k\,\gamma_{m,p,\ell}}, \tag{2}$$

with $\gamma_{m,p,\ell} = x_{p,\ell}\sin\theta_{m,p}\cos\phi_{m,p} + y_{p,\ell}\sin\theta_{m,p}\sin\phi_{m,p} + z_{p,\ell}\cos\theta_{m,p}$, $k = 2\pi/\lambda$ being the wave number, and λ being the wavelength. The angles $\theta_{m,p}$ and $\phi_{m,p}$ are, respectively, the elevation and azimuth associated with the direction of arrival (DOA) of the signal transmitted by the m^{th} source at node p.

Considering that node p applies the weight vector $\mathbf{w}_p = [w_{p,1}\ w_{p,2}\ \cdots\ w_{p,K_p}]^{\mathrm{T}}$, the beamforming output at snapshot n is given by

$$y[n] = \mathbf{w}^{\dagger}\,\mathbf{x}[n] = \mathbf{w}^{\dagger}\,\mathbf{A}\,\mathbf{s}[n] + \mathbf{w}^{\dagger}\,\mathbf{v}[n], \tag{3}$$

where $\mathbf{w} = [\mathbf{w}_1^{\mathrm{T}}\ \mathbf{w}_2^{\mathrm{T}}\ \cdots\ \mathbf{w}_P^{\mathrm{T}}]^{\mathrm{T}}$ is the concatenated weight vector and $(\cdot)^{\dagger}$ denotes the Hermitian transpose. Section III describes the centralized MPDR beamformer, which is used to obtain the optimal weight vector $\mathbf{w}$.

III. The Centralized MPDR Beamformer

The MPDR receiver beamformer [7] minimizes the array output power subject to a unity-gain constraint in the direction of the desired source. It is formulated as

$$\underset{\mathbf{w}}{\text{minimize}}\ \mathbf{w}^{\dagger}\mathbf{R}_{\mathbf{xx}}\mathbf{w} \quad \text{subject to} \quad \mathbf{w}^{\dagger}\mathbf{a}_m = 1, \tag{4}$$

where $\mathbf{w}$ denotes the beamforming weight vector, $\mathbf{R}_{\mathbf{xx}}$ is the covariance matrix of the received signals, assumed to be positive-definite, and $\mathbf{a}_m$ is the steering vector corresponding to the desired source or the signal of interest (SOI), for a given $m \in \{1, 2, \ldots, M\}$. The solution to this problem is

$$\mathbf{w} = \frac{\mathbf{R}_{\mathbf{xx}}^{-1}\mathbf{a}_m}{\mathbf{a}_m^{\dagger}\mathbf{R}_{\mathbf{xx}}^{-1}\mathbf{a}_m}, \tag{5}$$

which ensures the preservation of signals coming from the desired direction while minimizing interference and noise coming from other directions. In practice, the actual covariance matrix is unknown and replaced by its sample estimate

$$\widehat{\mathbf{R}}_{\mathbf{xx}} = \frac{1}{N}\sum_{n=0}^{N-1}\mathbf{x}[n]\mathbf{x}^{\dagger}[n], \tag{6}$$

where N is the number of snapshots.

The centralized MPDR beamformer for virtual arrays assumes a fusion node collecting raw data from all nodes to compute (5). This centralized approach involves extensive raw data exchange and significant computational complexity, mainly due to the inversion of $\mathbf{R}_{\mathbf{xx}}$. A computational complexity reduction proposed in [6] involves the use of the conjugate gradient (CG) method to directly compute $\mathbf{R}_{\mathbf{xx}}^{-1}\mathbf{a}_m$.

IV. The Distributed MPDR Beamformer

Distributed array signal processing techniques are particularly important when facing limited processing capabilities of nodes comprising the virtual array and restricted bandwidth for internode data exchanges, motivating the use of the distributed MPDR beamformer introduced in [6]. The distributed MPDR beamformer offers two primary advantages: (i) it significantly reduces internode communications by requiring only limited data exchange of ancillary variables rather than full-centralized processing with transmission of raw acquired data; and (ii) it lowers the computational complexity by enabling each node to process only its own received signals and compute its local weight vector $\mathbf{w}_p$ independently for $p \in \{1, 2, \ldots, P\}$. For a detailed analysis of computational complexity, see [6].

Algorithm 1 generalizes the distributed MPDR beamformer described in [6], employing an average consensus (AC) mechanism [8] to execute global operations without explicitly forming the full covariance matrix. Each node performs local

Algorithm 1 Distributed MPDR Beamformer

inputs: $\mathbf{a}_m$, $\{\mathbf{x}[n]\}_{n=0}^{N-1}$, K, N, P, ϵ
$\mathbf{e}_0 = \mathbf{a}_m$
$a_0 = \mathbf{e}_0^{\dagger}\,\mathbf{e}_0$
$\mathbf{d}_0 = \mathbf{e}_0$
$\mathbf{h}_0 = \mathbf{0}$
for $i = 0$ to $K-1$ **do**
  for $n = 0$ to $N-1$ **do**
    $t[n] = P \cdot \mathrm{AC}_p\left(\mathbf{x}_p^{\dagger}[n]\,\mathbf{d}_{i,p}\right)$
  end for
  for $p = 0$ to $P-1$ **do**
    $\mathbf{q}_{i,p} = \frac{1}{N}\sum_{n=0}^{N-1}\mathbf{x}_p[n]\,t[n]$
  end for
  $b_i = P \cdot \mathrm{AC}_p(\mathbf{d}_{i,p}^{\dagger}\,\mathbf{q}_{i,p})$
  $\alpha_i = a_i / b_i$
  for $p = 0$ to $P-1$ **do**
    $\mathbf{h}_{i+1,p} = \mathbf{h}_{i,p} + \alpha_i\,\mathbf{d}_{i,p}$
    $\mathbf{e}_{i+1,p} = \mathbf{e}_{i,p} - \alpha_i\,\mathbf{q}_{i,p}$
  end for
  $a_{i+1} = P \cdot \mathrm{AC}_p(\mathbf{e}_{i+1,p}^{\dagger}\,\mathbf{e}_{i+1,p})$
  if $a_{i+1} \le \epsilon$ **then**
    break ▷ Residual is sufficiently small
  end if
  $\beta_i = a_{i+1}/a_i$
  for $p = 0$ to $P-1$ **do**
    $\mathbf{d}_{i+1,p} = \mathbf{e}_{i+1,p} + \beta_i\,\mathbf{d}_{i,p}$
  end for
end for
$\mathbf{w} = \mathbf{h}_{i+1}/\mathbf{a}_m^{\dagger}\mathbf{h}_{i+1}$
return $\mathbf{w}$

computations based on its measurement vector $\mathbf{x}_p$, using average consensus to estimate global quantities like the inner products b_i and the residual norm a_i. These consensus-based estimates enable nodes to locally update intermediate solutions, residuals, and search directions within the CG method. Iterations continue until the consensus-based estimate of the residual norm a_{i+1} falls below a predefined threshold ϵ. Finally, a global normalization of the aggregated solution yields the weight vector. Therefore, the distributed algorithm utilizes average consensus to compute inner products locally, thereby facilitating a fully distributed CG implementation without the need to form the global covariance matrix explicitly.

In contrast to [6], the steering vector $\mathbf{a}_m$ is generalized to accommodate heterogeneous subarray geometries—configured in one, two, or three dimensions—with different numbers of antenna elements. Furthermore, unlike [6], the model presented in Section II assumes arbitrary node locations, explicitly accounting for potential grating lobes that arise when internode distances exceed $\lambda/2$ [9], which were not addressed in [6].

V. Performance Comparison

This section presents a numerical analysis of the theoretical MPDR (T-MPDR), centralized MPDR (C-MPDR), and distributed MPDR (D-MPDR). The T-MPDR was computed using (5), whereas C-MPDR and D-MPDR were obtained through numerical simulations based on Sections III and IV, respectively. To do so, we considered a single source ($M = 1$) emitting Gray-coded 4-phase shift keying (PSK) symbols with unit average power ($\sigma_{S_1}^2 = 1$), additive white Gaussian noise

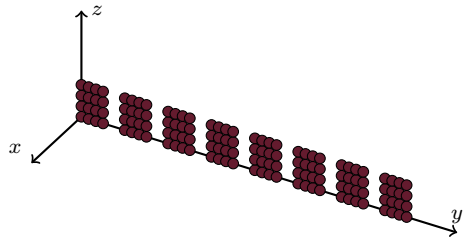

Fig. 2. Illustration of the homogeneous nodes in three-dimensional space.

($\sigma_V^2 = 0.1$), and $\epsilon = 10^{-8}$. Unless stated otherwise, the wavelength was normalized to $\lambda = 1$.

We considered 20 independent Monte Carlo trials to generate the numerical results. These simulations yielded quantities such as BER values and beam patterns, *i.e.*, $h(\theta,\phi) = \mathbf{w}^{\mathrm{T}}\mathbf{a}(\theta,\phi)$, with $\mathbf{a}(\theta,\phi)$ denoting a general steering vector composed of elements analogous to those in (2). Based on the beam pattern $h(\theta,\phi)$, both directivity and beam efficiency can be evaluated. These metrics are derived from the radiation intensity, which can be expressed by $U(\theta,\phi) = |h(\theta,\phi)|^2$. Consequently, the directivity is given by

$$D = \frac{4\pi U(\theta_m,\phi_m)}{\iint_{[0,4\pi]} U(\theta,\phi)\,\mathrm{d}\Omega}, \tag{7}$$

where $\mathrm{d}\Omega = \sin\theta\,\mathrm{d}\theta\,\mathrm{d}\phi$ and $U(\theta_m,\phi_m)$ is the maximum radiation intensity in the direction of arrival of $\mathbf{a}_m$. The beam efficiency is expressed as

$$\eta_{\text{beam}} = \frac{\iint_{\Omega_{\mathrm{ML}}} U(\theta,\phi)\,\mathrm{d}\Omega}{\iint_{[0,4\pi]} U(\theta,\phi)\,\mathrm{d}\Omega}, \tag{8}$$

where Ω_{ML} refers to the main lobe region. The remainder of this section is divided into two parts, presenting results for homogeneous and heterogeneous nodes.

A. Homogeneous nodes

A planar virtual array with eight nodes ($P = 8$), as illustrated in Fig. 2, was first simulated to assess the impact of grating lobes in a homogeneous configuration. Each node hosted a 4×4 rectangular subarray in the yz-plane, with internode spacings $d_{\text{inter}} \in \{\lambda/4, \lambda/2, 3\lambda/2\}$. Nodes were connected in a line-graph topology with sequential communication links. The distance between the elements of a subarray was $d = \lambda/2$ and the direction of arrival was fixed at an azimuth angle $\phi_{1,p} = 40^\circ$, $\forall\ p$ and elevation angle $\theta_{1,p} = 60^\circ$, $\forall\ p$.

Fig. 4 shows the overlaid normalized polar beam patterns for the three spacings, assuming the T-MPDR. For the smallest spacing ($d_{\text{inter}} = \lambda/4$), the array achieved a directivity of 19.92 dB with beam efficiency of 0.7561. At $d_{\text{inter}} = \lambda/2$, the directivity increased to 20.65 dB and the beam efficiency increased to 0.7843. For the largest internode spacing ($d_{\text{inter}} = 3\lambda/2$), the directivity achieved 20.73 dB whereas the beam efficiency dropped to 0.6481 due to significant energy leakage into grating lobes. These results indicate that, although increasing element spacing enhances directivity, it may exacerbate sidelobes, thus reducing beam efficiency.

The mean-squared error (MSE) convergence of D-MPDR compared to T-MPDR for $N \in \{10^3, 10^4, 10^5, 10^6\}$ is pre-

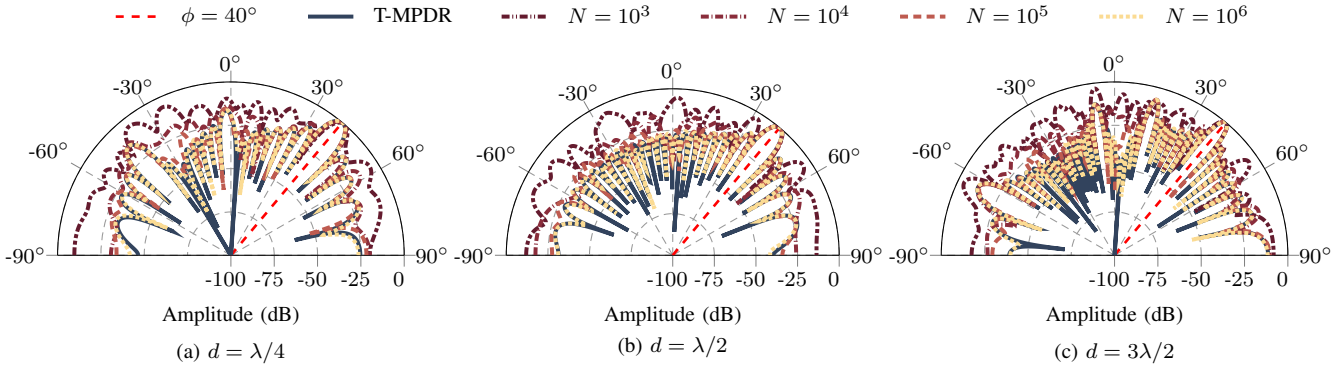

(a) $d = \lambda/4$ (b) $d = \lambda/2$ (c) $d = 3\lambda/2$

Fig. 3. Beam pattern of T-MPDR and D-MPDR as a function of ϕ in the plane $\theta = 60°$ with different N, assuming $d \in \{\lambda/4, \lambda/2, 3\lambda/2\}$.

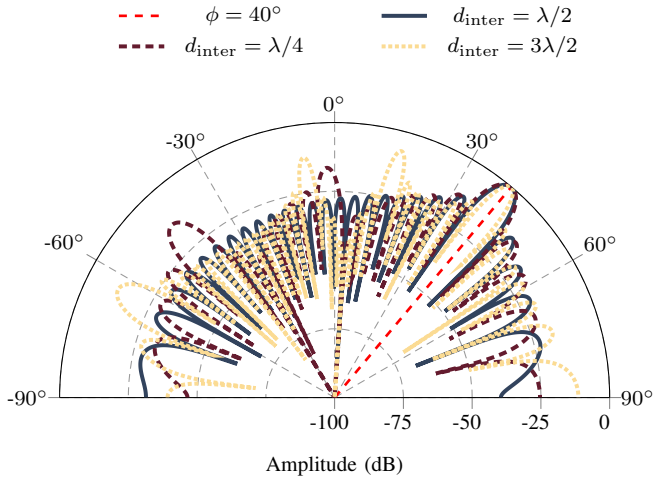

Fig. 4. Beam pattern of the T-MPDR as a function of ϕ in the plane $\theta = 60°$.

sented in Table I. Note that the number of snapshots had a greater influence on convergence than the variation of the internode spacing, emphasizing the need to accelerate the convergence rate.

Figs. 3(a)-(c) depict the polar beam patterns (in dB) in the azimuth plane at $\phi_{1,p} = 40°, \forall\ p$ for (a) $d_{\text{inter}} = \lambda/4$, (b) $d_{\text{inter}} = \lambda/2$, and (c) $d_{\text{inter}} = 3\lambda/2$. In each of the three subplots, four curves corresponding to different numbers of snapshots are overlaid to illustrate the convergence behavior of the D-MPDR. As the number of snapshots increased, the estimated beam patterns converged toward the theoretical MPDR response. Therefore, the number of snapshots was the primary driver of convergence, in agreement with the MSE results in Table I. Improvements must be introduced to reduce the necessary number of snapshots for convergence to a feasible one.

TABLE I

MSE FOR DIFFERENT ELEMENT SPACINGS AND NUMBER OF SNAPSHOTS

Number of snapshots	**MSE**		
	$\lambda/4$	$\lambda/2$	$3\lambda/2$
10^3	5.91×10^{-4}	5.98×10^{-4}	5.03×10^{-4}
10^4	4.67×10^{-5}	4.73×10^{-5}	4.69×10^{-5}
10^5	4.89×10^{-6}	5.08×10^{-6}	4.93×10^{-6}
10^6	4.44×10^{-7}	4.94×10^{-7}	4.14×10^{-7}

Figs. 5(a)–(c) show BER versus E_{b}/N_0 for T-MPDR and D-MPDR at various snapshot counts N. With $N = 10^3$, BER was highest—deviating significantly from the T-MPDR—due to poor covariance estimation. As N grows, the BER curves move closer to the ideal, and at $N = 10^6$ they overlap. Due to the considerable array gain, BER was nearly the same for all spacings d_{inter}. A comparison between D-MPDR and T-MPDR at a BER of 10^{-4} reveals approximate losses of 0.75 dB for $N = 10^6$, 4.34 dB for $N = 10^5$, 12.44 dB for $N = 10^4$ and 26.75 dB for $N = 10^3$. These values are in good agreement with Table I and underscore how the snapshot count strongly affects D-MPDR performance. In particular, the steep loss at $N = 10^3$ underscores the need to accelerate the convergence rate of D-MPDR. This behavior is attributed to the low network connectivity, as higher connectivity yields faster convergence.

B. Heterogeneous nodes

A virtual array of six heterogeneous nodes ($P = 6$), with $\lambda_1 = 8\lambda$ was considered in the simulations reported in this subsection. Each node employed a distinct subarray geometry, whose subarray parameters are listed in Table II. The nodes were positioned as illustrated in Fig. 6, meaning that $d_{\text{inter}} > \lambda_1/2$ for all nodes. The D-MPDR and C-MPDR were executed using $N = 10^6$ snapshots.

Fig. 7 displays the resulting polar beam patterns. In terms of directivity, T-MPDR achieved the highest directivity $D = 18.49$ dB, while the distributed implementation closely followed with $D = 18.13$ dB. The C-MPDR exhibited a modest degradation to $D = 18.07$ dB, reflecting the impact of processing all snapshots in a single node without internode

TABLE II

SUBARRAY GEOMETRIES AND PARAMETERS

Geometry	**Parameters**
Linear	$K_1 = 9$ and $d = \lambda_1/2$
Rectangular	$K_2 = 12$ and $d = \lambda_1/2$
Cube Surface	$K_3 = 26$ and $d = \lambda_1/2$
Elliptical	$K_4 = 15$, $a = \lambda_1$ and $b = \lambda_1/2$
Concentric Circular	$K_{5,r_1} = 6$, $K_{5,r_2} = 12$, $K_{5,r_3} = 16$, $r_1 = 3\lambda_1/2\pi$, $r_2 = 3\lambda_1/\pi$, $r_3 = 4\lambda_1/\pi$
Spherical	$K_6 = 40$ and $r = \lambda_1/2$

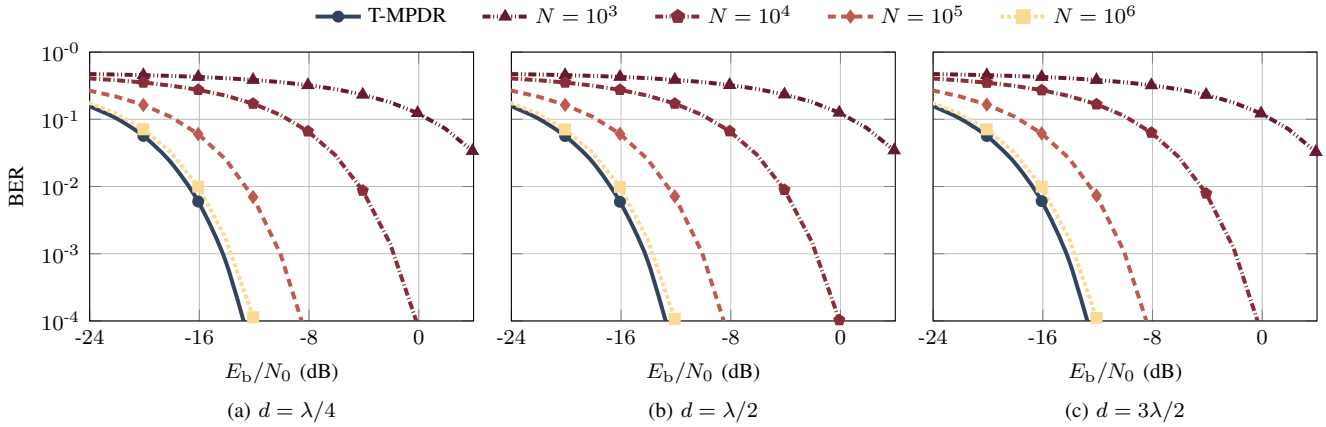

Fig. 5. BER versus E_b/N_0 for T-MPDR and D-MPDR with different N, assuming $d \in \{\lambda/4, \lambda/2, 3\lambda/2\}$.

cooperation. When examining beam efficiency, the distributed algorithm again approached the theoretical optimum ($\eta_{\text{beam}} = 0.3634$ vs. 0.3782 for T-MPDR), whereas the C-MPDR lagged at $\eta_{\text{beam}} = 0.3477$. These results show that the D-MPDR achieves near-theoretical directivity and efficiency, making it an attractive solution for virtual arrays constituted by heterogeneous nodes.

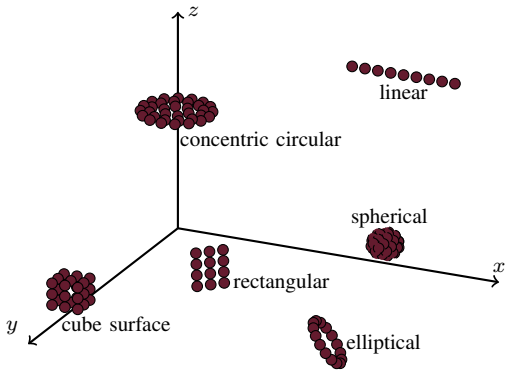

Fig. 6. Illustration of the heterogeneous nodes in three-dimensional space.

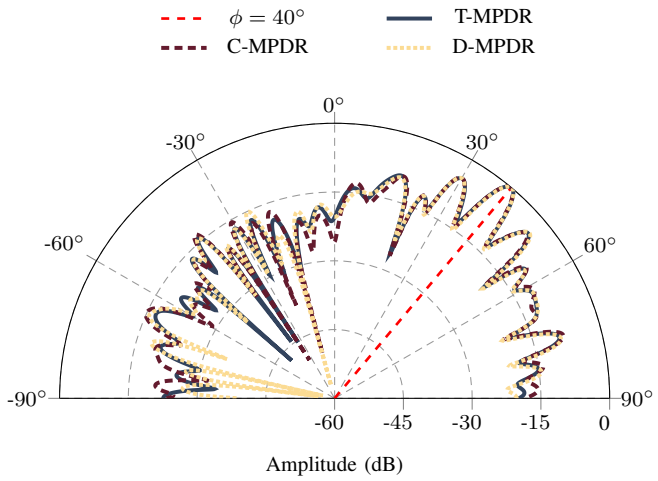

Fig. 7. Beam pattern of T-MPDR, C-MPDR, and D-MPDR as a function of ϕ in the plane $\theta = 60°$ for heterogeneous nodes.

VI. Conclusions

This paper generalized the distributed MPDR receiver beamformer for narrowband communications by using a virtual array composed of generic nodes in three-dimensional space, and compared it to its centralized MPDR counterpart. Internode spacings beyond $\lambda/2$ resulted in grating lobes in homogeneous node configurations. Furthermore, array gains could be traded off to keep the BER sufficiently low when the number of snapshots was small. Although the resulting distributed MPDR exhibited slow convergence, its performance approached the levels of its centralized counterpart with sufficient snapshots. In heterogeneous topologies, it remained robust to internode spacings beyond $\lambda/2$ due to the array gain. These findings confirm the advantages of further developing distributed array processing in virtual arrays. For future work, we aim to investigate the impact of network connectivity on the convergence and adaptive versions of the D-MPDR beamformer.

References

[1] E. Lagunas, S. Chatzinotas, and B. Ottersten, "Low-Earth orbit satellite constellations for global communication network connectivity," *Nature Reviews Electrical Engineering*, vol. 1, pp. 656–665, Oct. 2024.

[2] N. U. Hassan, C. Huang, C. Yuen, A. Ahmad, and Y. Zhang, "Dense small satellite networks for modern terrestrial communication systems: Benefits, infrastructure, and technologies," *IEEE Wireless Commun.*, vol. 27, no. 5, pp. 96–103, Oct. 2020.

[3] J. C. M. Duncan, V. N. Ha, J. Krivochiza, R. Palisetty, G. Eappen, J. A. Vasquez, W. A. Martins, S. Chatzinotas, and B. Ottersten, "Harnessing the power of swarm satellite networks with wideband distributed beamforming," in *IEEE 34th PIMRC*, Sep. 2023, pp. 1–6.

[4] D. Tuzi, T. Delamotte, and A. Knopp, "Satellite swarm-based antenna arrays for 6G direct-to-cell connectivity," *IEEE Access*, vol. 11, pp. 36 907–36 928, Mar. 2023.

[5] W. A. Martins, E. Lagunas, N. Skatchkovsky, F. Ortiz, G. Eappen, O. Simeone, B. Rajendran, and S. Chatzinotas, "Satellite adaptive onboard beamforming using neuromorphic processors," in *IEEE 35th PIMRC*, Sep. 2024, pp. 1–6.

[6] P.-C. Chen and P. P. Vaidyanathan, "Distributed algorithms for array signal processing," *IEEE Trans. Signal Process.*, vol. 69, pp. 4607–4622, Aug. 2021.

[7] H. L. Van Trees, *Optimum Array Processing: Part IV of Detection, Estimation, and Modulation Theory*. John Wiley & Sons, 2002.

[8] M. H. Degroot, "Reaching a consensus," *J. Am. Stat. Assoc.*, vol. 69, no. 345, pp. 118–121, Mar. 1974.

[9] D. Mestas, T. Delamotte, H. Legay, and A. Knopp, "Distributed array processing for multi-platform signal intelligence," in *IEEE MILCOM*, Oct. 2024, pp. 1–6.